LOC102553417 silencing facilitates the apoptosis of hepatic stellate cells via the miR-30e/MTDH axis

WUJUN WEI[1,2*], CHENG LIN[3*], RENTONG HU[1], JINGJING HUANG[4], XIAOHAO CHEN[1], LV ZHOU[1], JIAZHU WEI[1], YI-BIN DENG[1,2] and CHUN-FANG WANG[1]

[1]Center for Clinical Laboratory Diagnosis and Research; [2]Guangxi Clinic Medicine Research Center of Hepatobiliary Diseases; [3]Oncology Department, Affiliated Hospital of Youjiang Medical University for Nationalities; [4]Department of Health Medicine, Baise Maternal and Child Health Hospital, Baise, Guangxi Zhuang Autonomous Region 533000, P.R. China

Received April 11, 2022; Accepted August 5, 2022

DOI: 10.3892/mmr.2022.12865

Abstract. Hepatic fibrosis is an inevitable pathological process in the progression of multiple chronic liver diseases and remains a major challenge in the treatment of liver diseases. The purpose of the present study was to demonstrate whether silencing of the long non-coding RNA LOC102553417 promoted hepatic stellate cell (HSC) apoptosis via the microRNA (miR)-30e/metadherin (MTDH) axis. A LOC102553417 silencing lentivirus was constructed and transduced into HSC-T6 cells. After confirming the silencing efficiency by reverse transcription-quantitative PCR, cell proliferation was assessed using the Cell Counting Kit-8 assay and apoptosis was assessed using flow cytometry. The interaction between LOC102553417 and miR-30e, and that between miR-30e and MTDH, was demonstrated using the dual-luciferase reporter assay and RNA binding protein immunoprecipitation. The apoptosis of HSC-T6 cells was detected after transfection of miR-30e mimics and inhibitors with or without silencing LOC102553417. Silencing of LOC102553417 curbed HSC-T6 cell proliferation and expedited their apoptosis. LOC102553417 was demonstrated to target miR-30e, whereas miR-30e targeted MTDH. In addition, LOC102553417 silencing significantly upregulated miR-30e expression levels, and significantly downregulated MTDH mRNA and protein expression levels, which resulted in a significantly reduced p-Akt/Akt ratio and significantly elevated p53 protein expression levels. Transfection with miR-30e mimic alone significantly enhanced HSC-T6 cell apoptosis and inhibits LOC102553417 and MTDH expressions, In addition, miR-30e mimic expedites the apoptosis of HSCs stimulated by LOC102553417 silencing; consistent results were obtained by reverse validation of miR-30e inhibitor. In conclusion, the present study demonstrated that LOC102553417 silencing stimulated the apoptosis of HSCs via the miR-30e/MTDH axis.

Correspondence to: Professor Yi-Bin Deng, Guangxi Clinic Medicine Research Center of Hepatobiliary Diseases, Affiliated Hospital of Youjiang Medical University for Nationalities, 18 Zhongshan Second Road, Baise, Guangxi Zhuang Autonomous Region 533000, P.R. China
E-mail: dengyb75@163.com

Professor Chun-Fang Wang, Center for Clinical Laboratory Diagnosis and Research, Affiliated Hospital of Youjiang Medical University for Nationalities, 18 Zhongshan Second Road, Baise, Guangxi Zhuang Autonomous Region 533000, P.R. China
E-mail: chunfang.wang@ymun.edu.cn

*Contributed equally

Key words: long non-coding RNA LOC102553417, microRNA-30e, metadherin, hepatic stellate cell, hepatic fibrosis

Introduction

Hepatic fibrosis (HF) is an important health condition linked to chronic liver injury and HF is a disease associated with high morbidity (1). HF is a pathological process involving structural or functional abnormalities of the liver mainly attributed to the excessive accumulation of extracellular matrix components in hepatic tissues, which can lead to liver cirrhosis and liver cancer (2). The morbidity and mortality of HF-induced liver cirrhosis and liver cancer rank sixth globally and are increasing year-on-year in China (3). Previous studies reported that drugs for liver fibrosis treatment mainly inhibit hepatocyte apoptosis (emricasan) (4) and hepatic stellate cell (HSC) activation (PRI-724) (5), reduce fibrotic scar evolution and contraction (simtuzumab) (6), and regulate the immune response (cenicriviroc) (7). However, there is currently a lack of effective strategies and drugs to directly treat this disease (8,9). Numerous studies have demonstrated that the initiation and development of HF are primarily elicited by factors including viral infections, alcohol toxins and metabolites (Such as cholesterol). Furthermore, the activation and proliferation of HSCs also serve as key drivers of HF (10,11). HSC activation is a complicated process controlled by multiple molecules and signaling pathways (12), yet its underlying mechanisms remain largely undetermined. Exploring the molecular mechanisms related to the function of HSCs in order to identify new diagnostic and therapeutic molecular targets could be instrumental in developing new possibilities for the treatment of HF.

Long non-coding (lnc)RNAs are a set of non-protein-coding transcripts with a length of over 200 nt (13). A better understanding of HF could support the use of novel concepts and avenues in the targeted therapy of HF (14). A recent study by Zhang *et al* (15) reported that lnc-Lfar1 was closely associated with HF and modulated the macrophage activation evoked via lipopolysaccharide and IFN-γ to influence the occurrence and development of fibrosis via the NF-κB signaling pathway. Furthermore, Liao *et al* (16) recently reported that the lncRNA Gpr137b-ps could bind to and impair microRNA (miRNA/miR)-200a-3p causing inhibition of chemokine (C-X-C motif) ligand 14, which may promote the pathological process of HF via alteration of the activation and proliferation of HSCs. A whole-transcriptome sequencing analysis by Gong *et al* (17) revealed that lncRNA LOC102553417 (Genbank ID: XR_595047) was expressed at a high level in a rat carbon tetrachloride-induced HF model. LOC102553417 is a lncRNA of rats, which can be queried through the UCSC database (genome-asia.ucsc.edu). However, the role of LOC102553417 in the occurrence and development of HF remains undetermined. In the present study, LOC102553417 silencing was used to investigate its role in HSC activation via the miR-30e/metadherin (MTDH) axis. An in-depth understanding of the functions and mechanisms of LOC102553417 in HF could provide a theoretical basis for the clinical use of LOC102553417 as a diagnostic biomarker and treatment for HF.

Materials and methods

Culture of rat HSC-T6 cells. The rat HSC-T6 cell line was purchased from The Cell Bank of Type Culture Collection of The Chinese Academy of Sciences. Cells were cultured at 37˚C with 5% CO_2 in DMEM (cat. no. PM150210; Procell Life Science & Technology Co., Ltd.), which was supplemented with 10% fetal bovine serum (cat. no. 164210-500; Procell Life Science & Technology Co., Ltd.) and 1% penicillin-streptomycin (cat. no. PB180120; Procell Life Science & Technology Co., Ltd.). The cells were passaged at a 1:3 ratio and the medium was renewed three times per week. For TGF-β1 induction, HSC-T6 cells were stimulated with 10 ng/ml TGF-β1 (cat. no. HY-P7118; MedChemExpress) for 24 h at 37˚C or treated with an equal amount of double-distilled H_2O as the control.

Cell transduction and transfection. The LOC102553417 silencing lentiviral vector (vector no. GV492) was constructed by Guangzhou Anernor Biotechnology Co., Ltd. Briefly, GV492 plasmid vector (100 nM) and packaging plasmid (psPaX2; third generation lentiviral packaging system (vector: packaging vector: envelope ratio, 10:3:1; Promega Corporation) were mixed with lipo3000 (L3000-015; Invitrogen; Thermo Fisher Scientific, Inc.) were co-transfected into $1x10^6$ 293T cells (Cell Bank of the Chinese Academy of Sciences). When 293T cells were cultured for 4 days, the cell supernatant was collected, and then the collected cell supernatant was centrifuged at 251.55 x g for 5 min at 4˚C, and the supernatant was filtered with a 0.22 μm membrane. The targeting sequences used for the knockdowns (KDs) and negative control (NC, non-targeting.) were as follows: KD1, 5'-GACCCTGCATCA GAGTCTTCCAGA-3'; KD2, 5'-GGACTCTTCCTGGAC TACCATAAAT-3'; KD3, 5'-CATACATGCTAGGGCAGC CATTGCA-3'; and NC, 5'-TTCTCCGAACGTGTCACGT-3'. HSC-T6 cells were transduced at 37˚C (multiplicity of infection, 30) for 96 h and green fluorescence was observed via fluorescence microscopy to demonstrate transduction (data not shown). LOC102553417 expression was determined via reverse transcription-quantitative (RT-q)PCR. The vector with the highest silencing efficiency was used for subsequent experimentation at 24 h post-transduction.

The miR-30e mimic (sense, 5'-UGUAAACAUCCUUGA CUGGAAG-3', double chain; antisense 5'-CUUCCAGUC AAGGAUGUUUACA-3'), miR-30e inhibitor (5'-CUUCCA GUCAAGGAUGUUUACA-3'), mimic NC (5'-UUUGUACUA CACAAAAGUACUG-3') and inhibitor NC (5'-CAGUAC UUUUGUGUAGUACAAA-3') vectors were synthesized by Huzhou Hippo Biotechnology Co., Ltd. Lipofectamine® 3000 kit (cat. no. L3000015; Invitrogen; Thermo Fisher Scientific, Inc.) was employed for transfection(final concentration of nucleic acid: 20nM, cell density, 50%, 37˚C) for 48 h, subsequent experiments were performed 48 h after transfection.

RT-qPCR. TRIzol® reagent (cat. no. 15596-026; Invitrogen; Thermo Fisher Scientific, Inc.) was used to extract total cellular RNA. RT-PCR was performed using an RT-PCR kit (cat. no. RT-02011; Chengdu Foregene Biotechnology Co., Ltd.), which consisted of 10 μl SYBR-Green Mix, 2 μl forward (F) primer, 2 μl reverse (R) primer, 1 μl cDNA and 5 μl RNase-free deionized water. After the purity and concentration tests, RNA was reverse transcribed into cDNA (70˚C, 5 min; 42˚C, 60 min; 70˚C, 10 min). Primer Premier 5.0 software (Premier, Inc.) was employed for primer design; each primer was composed of 20-22 bases and the product size was 70-200 bp. The reaction conditions were set as follows: Pre-denaturation for 15 sec at 95˚C; 40 cycles of denaturation for 5 sec at 95˚C, annealing and extension at 60˚C for 30 sec; and for the melting curve, amplification at 55-95˚C for 10 sec (81 cycles in total). Three parallel wells were used for each group with a blank control and a NC group at the same time. After determining the cycle threshold, the relative expression of the target gene normalized to the internal control(GAPDH was used for lncRNA and mRNA, U6 was used for miRNA) was calculated using $2^{-\Delta\Delta Cq}$ analysis (18). The primer sequences were synthesized by Sangon Biotech Co., Ltd. as follows: LOC102553417 (F), AGTCCTGCCCACACT GCTTTT; LOC102553417 (R), AACAGAGGCCTGAAA TAGAC; MTDH (F), AGCGGGAGGAGGTGACCCCGCC; MTDH (R), ATTTGGTTTGGGCTTTTCA; miR-30e-RT, GTCGTATCCAGTGCAGGGTCCG AGGTATTCGCAC TGGATACGACCTTCCAGT; miR-30e (F), GCCGAGTGT AAACATCCT; miR-30e (R), GTCGTATCCAGTGCGAAT AC; GAPDH (F), TGTGAACGGATTTGGCCGTA; GAPDH (R), GATGGTGATGGGTTTCCCGT; U6 (F), CTCGCTTCG GCAGCACA; and U6 (R), AACGCTTCACGAATTTGCGT.

Western blotting. Cells were lysed using RIPA lysis buffer (cat. no. P0013B; Beyotime Institute of Biotechnology). Following homogenization, lysis and centrifugation at 200 x g for 5 min at 4˚C, total protein was extracted and the concentration was assessed using the BCA method. Following separation

via SDS-PAGE (5% stacking gel, 12% running gel, 20 μg total protein per lane). Electrophoresed proteins were transferred to a PVDF membrane (constant current of 200 mA for 1 h and a constant current of 250 mA for 2 h). The membrane was then blocked with TBS-Tween (Tween 0.1% in TBS) solution containing 5% skimmed milk powder for 1 h and was incubated with primary antibodies against the following proteins: Akt (1:500; cat. no. ab18785; Abcam), phosphorylated (p)-Akt (1:500; cat. no. ab8933; Abcam), p53 (1:333; cat. no. ab26; Abcam), MTDH (1:10,000; cat. no. ab124789; Abcam), β-actin (1:20,000; cat. no. 66009-1-Ig; ProteinTech Group, Inc.), Cleaved Caspase-3 (1:500; cat. no. ab32042; Abcam) and caspase-3 (1:1,000; cat. no. 19677-1-AP; ProteinTech Group, Inc.). After 1 h of agitation at room temperature, overnight incubation was performed with the primary antibodies at 4˚C. After washing, the membrane was incubated with a secondary antibody (HRP; anti-rabbit 1:5000, cat. no. 074-1506; anti-mouse 1:5000, cat. no. 074-1807; KPL, Inc.) for 1 h at 37˚C. The bands were visualized using ECL kit (P0018S; Beyotime Institute of Biotechnology), followed by pressing, exposure and fixation. Grayscale analysis of the images was performed using ImageJ software 1.8.0 (National Institutes of Health).

Cell Counting Kit-8 (CCK-8). HSC-T6 cell suspension was prepared and seeded onto a 96-well plate (100 μl/well) at 1x10^3 cells/well with three parallel wells for each group. On each of 5 consecutive days, 10 μl CCK-8 reagent (cat. no. FC101-03; TransGen Biotech Co., Ltd.) was added to each well. Following incubation in 37˚C and 5% CO_2 incubator for 2 h, absorbance was quantified at 450 nm using an ELx800 Absorbance Microplate Reader (BioTek Instruments Inc.).

Flow cytometry. HSC-T6 cells were transferred directly into a 10-ml centrifuge tube at 10^6/ml cells per sample, total 1ml. Following centrifugation at 200 x g for 5 min, the supernatant was discarded. Subsequently, cells (100 μl) were suspended in a 5 ml flow tube and incubated with 5 μl Annexin V-PE and 5 μl PI (cat. no. 640914; Biolegend, Inc.) at ambient temperature for 15 min. The samples were then loaded onto a CytoFLEX Flow Cytometer (Beckman Coulter, Inc.) for apoptosis analysis with FlowJo Software V10 (FlowJo, LLC).

Bioinformatics analysis of binding sites. It has been reported that miR-30e is a miRNA associated with HF using the RegRNA2 database (regrna2.mbc.nctu.edu.tw/) (19), predicted that wild-type (WT) LOC102553417 contained a binding site with miR-30e. The binding site was mutated into the original complementary sequence and designed as LOC102553417 mutant (MUT). The TargetScan database, version 8.0 (http://www.targetscan.org/vert_80/) was used to identify potential target genes selecting the total context++ score <-0.8, aggregate P_{CT} ≥90 and selecting for genes that have been reported to be related to liver disease. miR-30e was predicted to have a binding site with MTDH and based on the binding site, the binding site was mutated into the original complementary sequence and designed as MTDH MUT.

Dual-luciferase reporter assay. Log-phase HSC-T6 cells were seeded into a 24-well plate and cultured for 24 h. Cell transfection by lipo3000 (L3000-015; Invitrogen; Thermo Fisher Scientific, Inc.) was performed using MTDH 3'UTR or LOC102553417 (wild or mutant type) psicheck2 luciferase reporter gene plasmid (Shanghai Genechem Technology Co., Ltd), *Renilla* control plasmid, aforementioned miR-30e mimic or mimic-NC. Three parallel wells were used in each group. After culture at 37˚C and 5% CO_2 for 24 h, the medium was discarded and the residual medium was removed via two washes in ice-cold PBS. Immediately following transduction, activity measurement was performed. According to the manufacturers' protocol, 100 μl 1X Passive Lysis Buffer from the Dual-Luciferase Reporter Assay System kit (cat. no. E1910; Promega Corporation) was added to each well. Following gentle shaking, the cells were maintained at ambient temperature for 15 min. The lysate (20 μl) was placed into a 96-well plate and the luminescence was quantified using a Lux-T020 Ultra-sensitive Tube Luminometer (Guangzhou Biolight Biotechnology Co., Ltd.) for statistical analysis of relative luciferase activity normalized to *Renilla* luciferase activity.

RNA-binding protein immunoprecipitation (RIP). According to the manufacturer's instructions of RIP kit (cat. no. Bes5101; Guangzhou Boxin Biotechnology Co., Ltd.), RIP buffer and Argonaute RNA-induced silencing complex catalytic component 2 (Ago2) antibodies 3ug (cat. no. ab233727; Abcam) were equilibrated at ambient temperature for 10 min. The harvested HSC-T6 cells were lysed with RIP lysis buffer at 4˚C for 10 min, washed with 2 ml PBS and centrifuged at 200 x g for 5 min at room temperature to collect cell lysate. The cell lysate (100 μl) was incubated with RIP buffer (900 μl) containing antibody-labeled A + G magnetic beads (20 μl) at 4˚C for 16 h (overnight). IgG (cat. no. ab172730; Abcam) served as a NC and the supernatant was harvested as 'Input' as a control. The immunoprecipitated complex was isolated and detached with 150 μl proteinase K buffer to isolate the RNA at 55˚C for 1 h. RT-qPCR was employed to analyze the relative expression of miR-30e and LOC102553417 as aforementioned.

Statistical analysis. All experimental data were analyzed using Prism 8.0 software (GraphPad Software Inc.). Statistics was obtained from three repeat experiments. Data are presented as the mean ± standard deviation. Comparisons between two groups were performed using unpaired Student's t-test, whereas one-way ANOVA followed by Tukey's post-hoc test was used for comparisons among three or more groups. $P<0.05$ was considered to indicate a statistically significant difference.

Results

LOC102553417 silencing decreases HSC-T6 cell proliferation and increases their apoptosis. To ascertain the importance of LOC102553417 in the activation of HSCs, the mRNA expression levels of LOC102553417 after TGF-β1-triggered activation of HSC-T6 cells were determined using RT-qPCR. LOC102553417 mRNA expression levels in the TGF-β1-induced group were significantly higher compared with those in the control group ($P<0.001$; Fig. 1A). Post-transduction of HSC-T6 cells with LOC102553417 silencing vectors and NC vector, LOC102553417 mRNA expression levels were assessed via RT-qPCR. The mRNA expression levels of LOC102553417 in the KD1 group

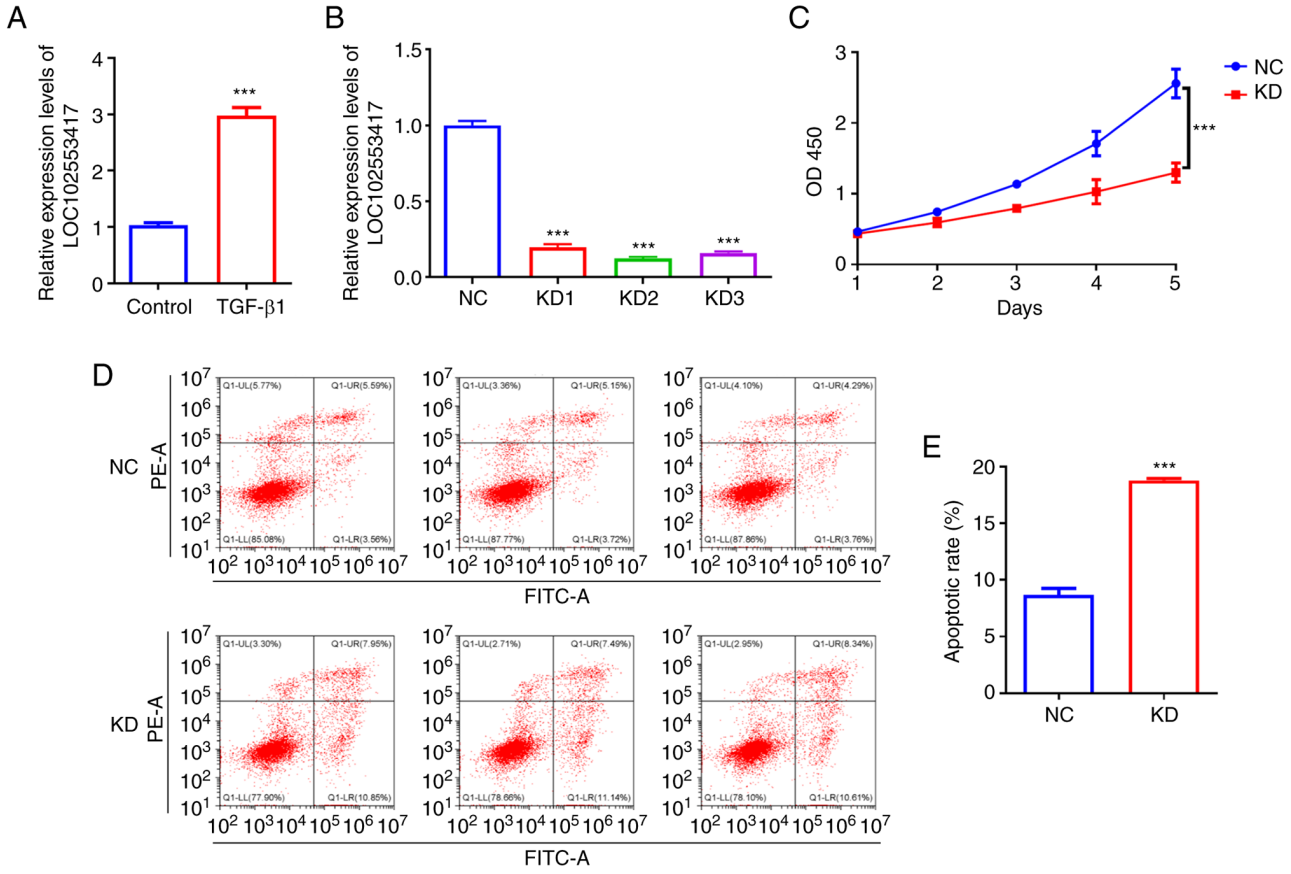

Figure 1. LOC102553417 silencing limits HSC-T6 cell proliferation and their resistance to apoptosis. (A) LOC102553417 expression in TGF-β1-activated HSC-T6 cells was assessed via RT-qPCR. (B) Transfection efficiency of LOC102553417 KD vectors in HSC-T6 cells presented as mRNA expression levels was assessed via RT-qPCR. (C) Proliferation of HSC-T6 cells was assessed via Cell Counting Kit-8 assay following LOC102553417 silencing. (D) Flow cytometry dot plots and (E) statistical analysis of the apoptotic rate of HSC-T6 cells following LOC102553417 silencing. Results are expressed as the mean ± SD (n=3). ***P<0.001. RT-qPCR, reverse transcription-quantitative PCR; NC, negative control; KD, knockdown; OD, optical density.

(0.20±0.02), KD2 group (0.12±0.01) and KD3 group (0.16±0.01) were all significantly downregulated compared with those in the NC vector group (1.00±0.03; P<0.001). The silencing efficiency of LOC102553417 KD2 was the greatest (Fig. 1B); therefore, KD2 was selected for use in the subsequent experiments. CCK-8 assay demonstrated significantly reduced proliferation of HSCs in LOC102553417-silenced cells compared with in the NC group (P<0.001; Fig. 1C). Furthermore, flow cytometry data demonstrated increased cell apoptosis in LOC102553417-silenced cells compared with in the NC group (P<0.001; Fig. 1D and E).

LOC102553417 competitively binds to miR-30e, which upregulates MTDH expression. Using the RegRNA2 database predicted that wild-type (WT) LOC102553417 contained a binding site with miR-30e. MUT LOC102553417 was designed (Fig. 2A. Using the TargetScan predicted that WT MTDH 3'UTR contained a binding site with miR-30e. MUT MTDH 3'UTR was designed (Fig. 2B).

The binding of LOC102553417 to miR-30e was demonstrated by the dual-luciferase reporter assay. Luciferase activity was significantly reduced in the LOC102553417-WT + miR-30e mimic compared with that in the LOC102553417-WT + miR-NC group (P<0.01; Fig. 2C). However, the LOC102553417-MUT + miR-30e mimic demonstrated no significant difference in luciferase activity compared with the LOC102553417-MUT + miR-NC group (P>0.05), which demonstrated the binding of LOC102553417 to miR-30e at the aforementioned binding site. The binding of MTDH to miR-30e was also demonstrated using the luciferase assay. Compared with the MTDH-WT + miR-NC group, the MTDH-WT + miR-30e mimic group demonstrated significantly reduced luciferase activity (P<0.01); however the MTDH-MUT + miR-30e mimic group demonstrated no significant difference in luciferase activity compared with the MTDH-MUT + miR-NC group (P>0.05; Fig. 2D), which demonstrated the binding of miR-30e to MTDH at the binding site predicted using TargetScan database.

Antibodies to Ago2, a miRNA precursor cleavage protein, were used to conduct RIP experiments to verify the binding of miR-30e to LOC102553417. Compared with in the IgG antibody group (NC antibody), significantly higher expression levels of miR-30e and LOC102553417 were detected in the Ago2 antibody group (P<0.001; Fig. 2E). Subsequently, LOC102553417 was silenced in HSC-T6 cells, the miR-30e and MTDH expression levels were determined via RT-qPCR, and the MTDH protein expression levels were assessed via western blotting. miR-30e relative expression levels in the KD group were significantly elevated compared with those in the NC group (P<0.001; Fig. 2F). MTDH mRNA expression levels (P<0.001; Fig. 2G)

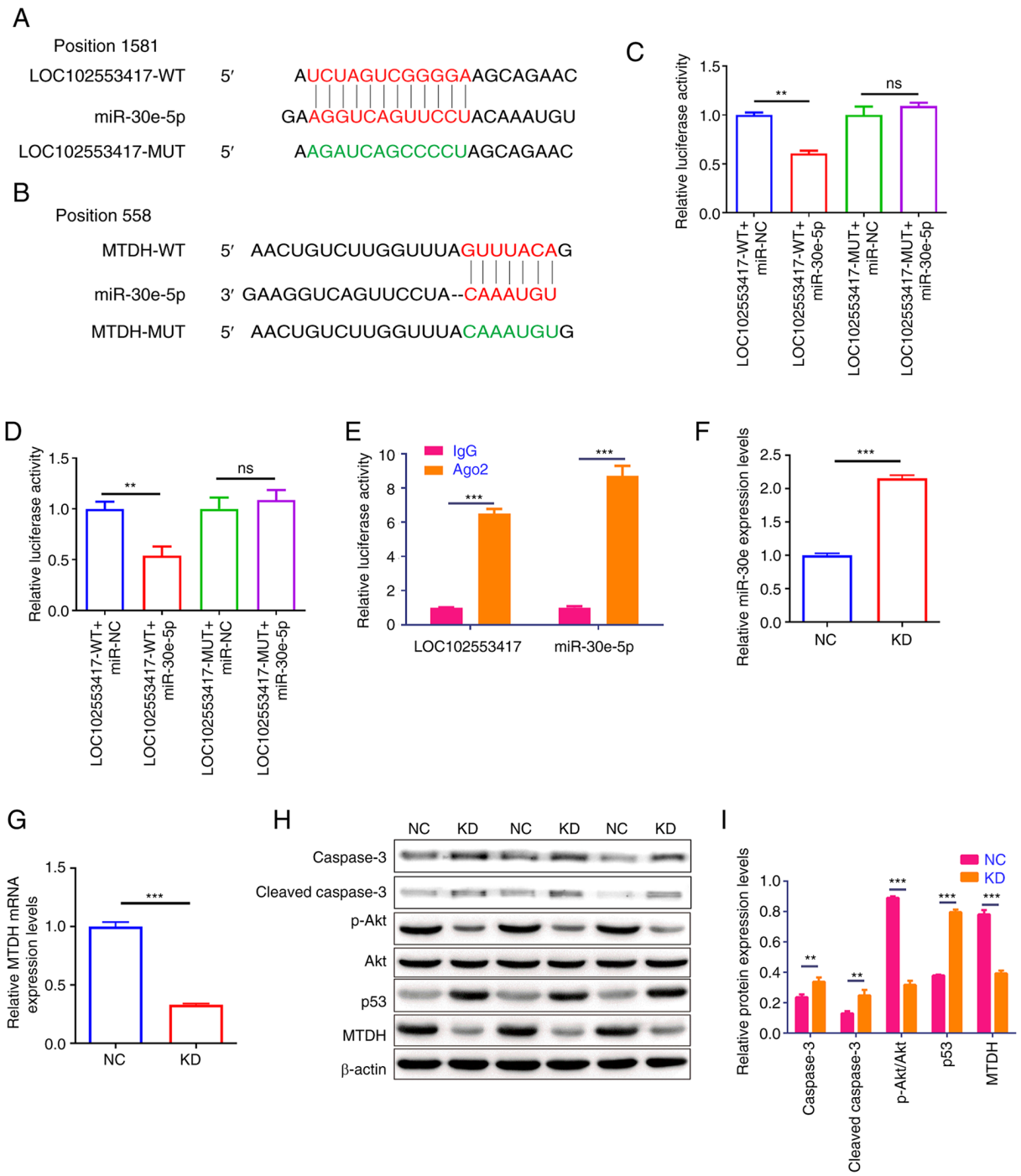

Figure 2. LOC102553417 silencing suppresses MTDH expression via competitively binding to miR-30e. Alignment of the binding site between (A) LOC102553417, miR-30e and the designed MUT sequence, and (B) miR-30e, MTDH and the designed MUT sequence. Binding of (C) miR-30e to LOC102553417 and (D) miR-30e to MTDH were assessed via dual-luciferase reporter assay. (E) Binding of miR-30e to LOC102553417 was assessed via RNA binding protein immunoprecipitation. mRNA expression levels of (F) miR-30e and (G) MTDH were assessed via RT-qPCR. (H) Representative western blotting images of MTDH, Akt, p-Akt, p53, caspase-3 and cleaved caspase-3 protein bands. (I) Statistical analysis of MTDH, Akt, p-Akt, p53, caspase-3 and cleaved caspase-3 protein expression levels assessed via western blotting. Results are expressed as the mean ± SD (n=3). **P<0.01; ***P<0.001; ns, no significant difference; WT, wild-type; MUT, mutant; NC, negative control; Ago2, Argonaute RNA-induced silencing complex catalytic component 2; p, phosphorylated; miR, microRNA; MTDH, metadherin; RT-qPCR, reverse transcription-quantitative PCR; NC, negative control; KD, knockdown.

and protein expression levels (P<0.001; Fig. 2H and I) were significantly reduced in the LOC102553417 KD group compared with those in the NC group. Western blot analysis of the protein expression levels of p-Akt, Akt, caspase-3, cleaved caspase-3 and p53 was used to assess the downstream mechanism of the LOC102553417/miR-30e/MTDH axis. Western blotting demonstrated significant reductions in the p-Akt/Akt ratio (P<0.001), and significant elevations in p53, caspase-3 and cleaved caspase-3 protein expression levels (P<0.001) in the LOC102553417 KD group compared with those in the NC group.

miR-30e inhibits LOC102553417 and MTDH expression levels and expedites the apoptosis of HSCs in which LOC102553417 is knocked down. The present study subsequently focused

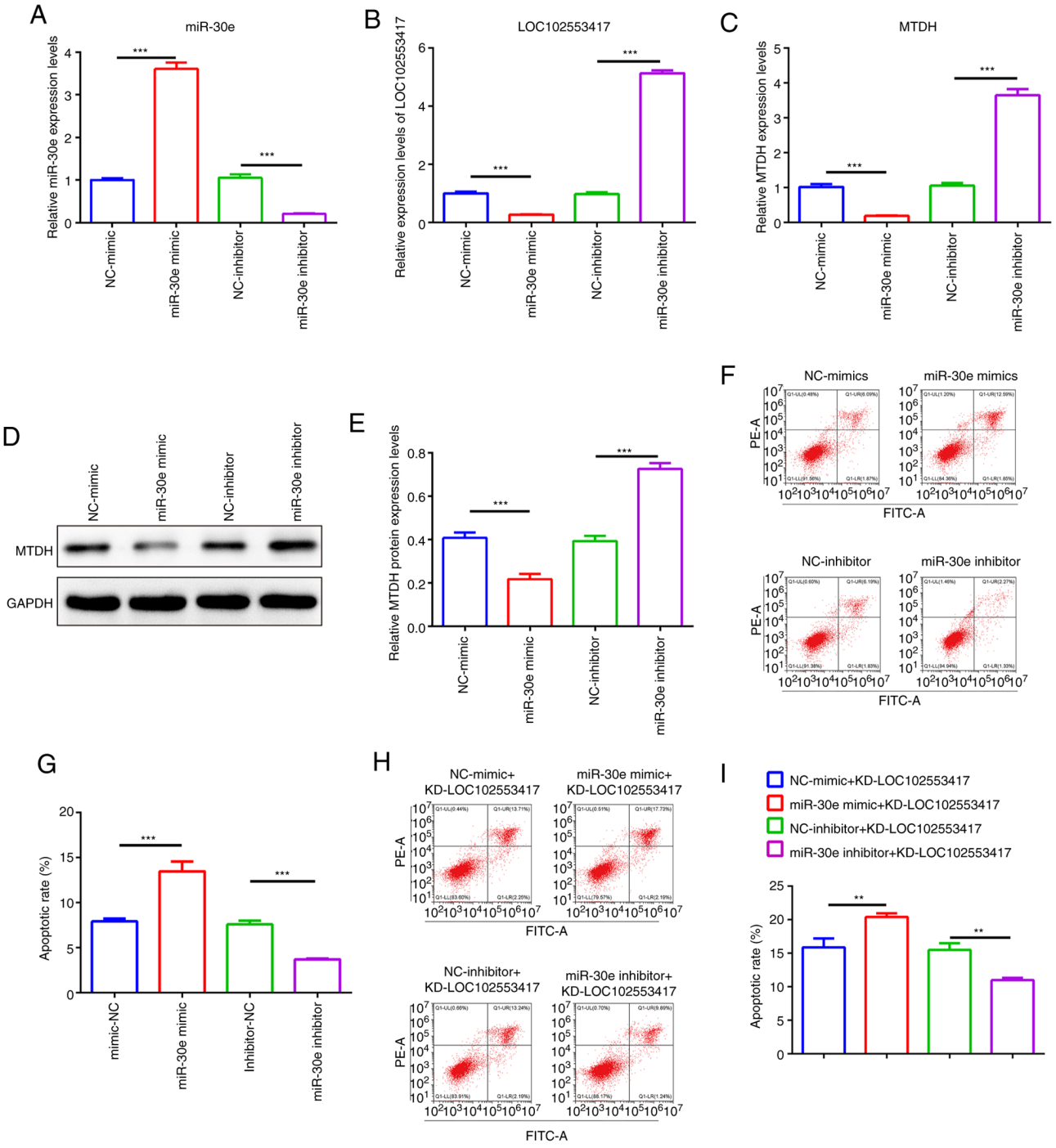

Figure 3. miR-30e suppresses LOC102553417 and MTDH and accelerates the apoptosis of HSC-T6 cells evoked by LOC102553417 deficiency. Quantification of expression levels of (A) miR-30e, (B) LOC102553417 and (C) MTDH via RT-qPCR. (D) Representative western blotting images of MTDH protein bands. (E) Statistical analysis of MTDH protein expression levels. (F) Representative flow cytometry dot plots and (G) statistical analysis of HSC-T6 cell apoptotic rate after treatment with miR-30e mimic or inhibitor. (H) Representative flow cytometry dot plots and (I) statistical analysis of HSC-T6 cell apoptotic rates after co-manipulation with miR-30e mimic or inhibitor and KD-LOC102553417. Results are expressed as the mean ± SD (n=3). **P<0.01 and ***P<0.001. RT-qPCR, reverse transcription-quantitative PCR; NC, negative control; KD, knockdown; MTDH, metadherin; miR, microRNA.

on whether LOC102553417 could function via the miR-30e/MTDH axis. miR-30e mimic, miR-30e inhibitor, NC-mimic and NC-inhibitor were constructed and transfected into HSC-T6 cells, and the mRNA expression levels of miR-30e, LOC102553417 and MTDH were quantified via RT-qPCR. miR-30e expression levels in the miR-30e inhibitor group were significantly reduced compared with those in the NC-inhibitor group (P<0.001; Fig. 3A); however, LOC102553417 (Fig. 3B) and MTDH (Fig. 3C) expression levels were significantly increased in the miR-30e inhibitor group compared with in the NC-inhibitor group (P<0.001). miR-30e mRNA expression levels were significantly raised in the miR-30e mimic group compared with in the NC-mimic group (P<0.001). Furthermore, the miR-30e mimic resulted in significant reductions in LOC102553417 and MTDH mRNA expression levels compared with in the NC-mimic group (P<0.001).

Western blotting demonstrated that MTDH protein expression levels were significantly elevated in the miR-30e inhibitor group compared with in the NC-inhibitor group (P<0. 001;Fig.3D and E); however, they were significantly reduced in the miR-30e mimic group compared with in the NC-mimic group (P<0.001) (Fig. 3D and E). Apoptosis analysis demonstrated that the apoptotic rate was significantly suppressed following miR-30e inhibitor transfection compared with that in the NC-inhibitor group (P<0.001; Fig. 3F and G). Furthermore, a significant increase in apoptotic rate was demonstrated after miR-30e mimic transfection compared with the NC-mimic (P<0.001). Compared with LOC102553417 silencing (NC-inhibitor + KD-LOC102553417), simultaneous miR-30e inhibitor and LOC102553417 silencing (miR-30e inhibitor + KD-LOC102553417) demonstrated a significantly reduced apoptotic rate (P<0.001), whereas simultaneous miR-30e mimic and LOC102553417 silencing (miR-30e mimic + KD-LOC102553417) demonstrated a significant enhancement in the apoptotic rate compared with NC-mimic + KD-LOC102553417 (P<0.001) (Fig. 3H and I). These findings indicate miR-30e inhibits LOC102553417 and MTDH expression levels and expedites the apoptosis of HSCs in which LOC102553417 is knocked down.

Discussion

HF is a dynamic process that manifests through extracellular matrix accumulation triggered by chronic liver injury of any etiology, including viral infection, alcoholic liver disease and nonalcoholic steatohepatitis (12). Activation of HSCs is a crucial event in HF, and their proliferation and apoptosis are highly relevant to the initiation and development of HF (20). Previous studies have reported that the proliferation of HSCs can drive the initiation of HF and stimulating HSC apoptosis could ameliorate HF (21,22). The present study demonstrated that silencing LOC102553417 contributed to the significant suppression of HSC-T6 cell proliferation and the significant enhancement of their apoptotic rate. Therefore, it could be hypothesized that LOC102553417 may be a driver of HF, which agrees with a previous finding that LOC102553417 was highly expressed in a rat model of HF (17), and that targeting LOC102553417 could be a potential strategy to treat HF.

The gene encoding MTDH is located on the long arm of human chromosome 8 (8q22) in region 22, with a molecular weight of ~64 kDa and has previously been reported as an miR-30e-5p target gene (23). MTDH can facilitate hepatocarcinogenesis and cancer progression (24); in addition, abnormal expression of miR-30a-5p can impede the proliferative function of liver cancer cells and enhance their apoptosis via targeting of the MTDH/PTEN/AKT pathway (25). MTDH knockout has been shown to impair the proliferation and accelerate the apoptosis of hepatocellular carcinoma cells via the PTEN/AKT pathway (26); however, the significance of MTDH in HF is rarely reported. Previous studies have reported that miR-30e is abnormally expressed in liver injury and hepatocellular carcinoma (27,28). Furthermore, hepatitis B virus X protein may promote the development of liver fibrosis and hepatoma through the downregulation of miR-30e, which targets prolyl 4-hydroxylase subunit α2 (29). Moreover, human antigen R has been reported to be involved in sphingosine 1-phosphate (S1P)-induced bone marrow mesenchymal stem cell migration and can increase the stabilization of S1P receptor 3 mRNA by competing with miR-30e to regulate liver fibrosis (30). The present study demonstrated that LOC102553417 loss-of-function expedited HSC apoptosis by inhibiting MTDH expression through competitively binding to miR-30e, which could be a key mechanism responsible for the action of LOC102553417 on HSCs, which drive HF. The combination of the miR-30e inhibitor and KD-LOC102553417 significantly inhibited apoptosis. The results of the present study demonstrated that the miR-30e inhibitor significantly decreased the apoptotic rate and that silencing of LOC102553417 significantly promoted apoptosis. Furthermore, miR-30e could competitively bind to LOC102553417 and when the miR-30e inhibitor inhibited the expression of miR-30e, thus reducing the binding of miR-30e to LOC102553417, the expression of LOC102553417 was significantly increased and the cell apoptotic rate was significantly reduced. Moreover, miR-30e inhibits LOC102553417 and MTDH expression levels, and expedites the apoptosis of HSCs in which LOC102553417 is knocked down. These results further indicate that the three factors have a mutual regulatory relationship in the apoptosis of hepatic stellate cells.

Akt is a serine/threonine protein kinase. Activation of the Akt signaling pathway mainly depends on the activity of PI3K, which can be stimulated by JAK1 and CD19. Akt phosphorylation is essential for Akt activation and subsequent PI3K/Akt signaling pathway activation (31-33). Akt phosphorylates downstream targets to block cell apoptosis (34). A recent study reported that activation of the PI3K/AKT/MDM2 signaling pathway could degrade p53, inhibiting apoptosis (35). p53 is a key tumor suppressor that suppresses cell proliferation and induces apoptosis. It predominantly maintains body homeostasis via diverse regulatory mechanisms, including mediating DNA repair, impeding cell proliferation, stimulating apoptosis and boosting metabolism (36,37). The results of the present study demonstrated that LOC102553417 silencing significantly increased apoptotic rate, significantly reduced Akt protein phosphorylation and significantly upregulated p53 protein expression levels. Furthermore, the present study demonstrated that LOC102553417 silencing could enhance Akt protein phosphorylation via the miR-30e/MTDH signaling pathway. This may be the downstream pathway of the LOC102553417-mediated miR-30e/MTDH axis affecting the apoptosis of HSCs.

Notably, the present study has certain limitations. Firstly, the significantly upregulated LOC102553417 expression in clinical HF samples and its clinical significance were not verified. Furthermore, the present study was only performed on rat HSCs and needs to be further explored and verified in human cells and clinical samples. Secondly, an HF cell model was not established to validate the *in vivo* function and mechanism of LOC102553417. Thirdly, pathway inhibitors were not utilized to verify the downstream pathways of the LOC102553417/miR-30e/MTDH axis; therefore, an in-depth exploration of their interaction is warranted in the future.

In conclusion, the present study demonstrated that silencing LOC102553417 reinforced HSC apoptosis via the miR-30e/MTDH axis, which could be a crucial regulatory mechanism in HF and may provide a theoretical basis for HF-targeted therapy.

Acknowledgements

Not applicable.

Funding

The present study was supported by The 2021 Young and Middle-aged Backbone Talents Research Project of the Affiliated Hospital of Youjiang Medical University for Nationalities (grant no. Y20212603), the National Natural Science Foundation of China (grant nos. 81460123 and 81960303), the Natural Science Foundation of Guangxi (grant no. 2018GXNSFAA281187), the Clinic Medicine Research Center of Hepatobiliary Diseases of Guangxi (grant no. AD17129025), the University-level Scientific Research Project of Youjiang Medical University for Nationalities (grant no. yy2019ky008), the Self-funded Scientific Research Project of Guangxi Zhuang Autonomous Region Health Committee (grant no. 20190953) and the Development Program Project of Baise City Scientific Research and Technology (grant no. Encyclopedia 20213242).

Availability of data and materials

The datasets used and/or analyzed during the current study are available from the corresponding author on reasonable request.

Authors' contributions

WW wrote the draft and designed the experiments. CL performed cell transfection. RH performed bioinformatics analysis and reviewed and edited the manuscript. JH performed vector design and RT-PCR and reviewed and edited the manuscript. XC performed western blotting. LZ performed Cell Counting Kit-8 assay. JW performed flow cytometry. YBD acquired funding, completed RIP and dual-luciferase assay, edited the manuscript and provided critical discussion. CFW analyzed data and acquired funding. WW and CFW confirm the authenticity of all the raw data. All authors read and approved the final manuscript.

Ethics approval and consent to participate

Not applicable.

Patient consent for publication

Not applicable.

Competing interests

The authors declare that they have no competing interests.

References

1. Roehlen N, Crouchet E and Baumert TF: Liver fibrosis: Mechanistic concepts and therapeutic perspectives. Cells 9: 875, 2020.
2. Lee YA, Wallace MC and Friedman SL: Pathobiology of liver fibrosis: A translational success story. Gut 64: 830-841, 2015.
3. Konyn P, Ahmed A and Kim D: Current epidemiology in hepatocellular carcinoma. Expert Rev Gastroenterol Hepatol 15: 1295-1307, 2021.
4. Harrison SA, Goodman Z, Jabbar A, Vemulapalli R, Younes ZH, Freilich B, Sheikh MY, Schattenberg JM, Kayali Z, Zivony A, *et al*: A randomized, placebo-controlled trial of emricasan in patients with NASH and F1-F3 fibrosis. J Hepatol 72: 816-827, 2020.
5. Kimura K, Ikoma A, Shibakawa M, Shimoda S, Harada K, Saio M, Imamura J, Osawa Y, Kimura M, Nishikawa K, *et al*: Safety, Tolerability, and preliminary efficacy of the anti-fibrotic small molecule PRI-724, a CBP/β-catenin inhibitor, in patients with hepatitis C virus-related cirrhosis: A single-center, open-label, dose escalation phase 1 trial. EBioMedicine 23: 79-87, 2017.
6. Muir AJ, Levy C, Janssen HLA, Montano-Loza AJ, Shiffman ML, Caldwell S, Luketic V, Ding D, Jia C, McColgan BJ, *et al*: Simtuzumab for primary sclerosing cholangitis: Phase 2 study results with insights on the natural history of the disease. Hepatology 69: 684-698, 2019.
7. Friedman SL, Ratziu V, Harrison SA, Abdelmalek MF, Aithal GP, Caballeria J, Francque S, Farrell G, Kowdley KV, Craxi A, *et al*: A randomized, placebo-controlled trial of cenicriviroc for treatment of nonalcoholic steatohepatitis with fibrosis. Hepatology 67: 1754-1767, 2018.
8. Friedman SL: Hepatic fibrosis: Emerging therapies. Dig Dis 33: 504-507, 2015.
9. Altamirano-Barrera A, Barranco-Fragoso B and Méndez-Sánchez N: Management strategies for liver fibrosis. Ann Hepatol 16: 48-56, 2017.
10. Higashi T, Friedman SL and Hoshida Y: Hepatic stellate cells as key target in liver fibrosis. Adv Drug Del Rev 121: 27-42, 2017.
11. Coll M, Perea L, Boon R, Leite SB, Vallverdú J, Mannaerts I, Smout A, El Taghdouini A, Blaya D, Rodrigo-Torres D, *et al*: Generation of hepatic stellate cells from human pluripotent stem cells enables in vitro modeling of liver fibrosis. Cell Stem Cell 23: 101-113.e107, 2018.
12. Tsuchida T and Friedman SL: Mechanisms of hepatic stellate cell activation. Nat Rev Gastroenterol Hepatol 14: 397-411, 2017.
13. Fathizadeh H, Hayat SMG, Dao S, Ganbarov K, Tanomand A, Asgharzadeh M and Kafil HS: Long non-coding RNA molecules in tuberculosis. Int J Biol Macromol 156: 340-346, 2020.
14. Peng H, Wan LY, Liang JJ, Zhang YQ, Ai WB and Wu JF: The roles of lncRNA in hepatic fibrosis. Cell Biosci 8: 63, 2018.
15. Zhang K, Shi Z, Zhang M, Dong X, Zheng L, Li G, Han X, Yao Z, Han T and Hong W: Silencing lncRNA Lfar1 alleviates the classical activation and pyoptosis of macrophage in hepatic fibrosis. Cell Death Dis 11: 132, 2020.
16. Liao J, Zhang Z, Yuan Q, Liu Q, Kuang J, Fang Y and Hu X: A lncRNA Gpr137b-ps/miR-200a-3p/CXCL14 axis modulates hepatic stellate cell (HSC) activation. Toxicol Lett 336: 21-31, 2021.
17. Gong Z, Tang J, Xiang T, Lin J, Deng C, Peng Y, Zheng J and Hu G: Genome-wide identification of long noncoding RNAs in CCl4-induced liver fibrosis via RNA sequencing. Mol Med Rep 18: 299-307, 2018.
18. Livak KJ and Schmittgen TD: Analysis of relative gene expression data using real-time quantitative PCR and the 2(-Delta Delta C(T)) Method. Methods 25: 402-408, 2001.
19. Chang TH, Huang HY, Hsu JB, Weng SL, Horng JT and Huang HD: An enhanced computational platform for investigating the roles of regulatory RNA and for identifying functional RNA motifs. BMC Bioinformatics 14 (Suppl 2): S4, 2013.
20. Wei S, Wang Q, Zhou H, Qiu J, Li C, Shi C, Zhou S, Liu R and Lu L: miR-455-3p alleviates hepatic stellate cell activation and liver fibrosis by suppressing HSF1 expression. Mol Ther Nucleic Acids 16: 758-769, 2019.
21. Seki E and Brenner DA: Recent advancement of molecular mechanisms of liver fibrosis. J Hepatobiliary Pancreat Sci 22: 512-518, 2015.
22. Shan L, Liu Z, Ci L, Shuai C, Lv X and Li J: Research progress on the anti-hepatic fibrosis action and mechanism of natural products. Int Immunopharmacol 75: 105765, 2019.
23. Zhang Z, Qin H, Jiang B, Chen W, Cao W, Zhao X, Yuan H, Qi W, Zhuo D and Guo H: miR-30e-5p suppresses cell proliferation and migration in bladder cancer through regulating metadherin. J Cell Biochem 120: 15924-15932, 2019.
24. Sarkar D: AEG-1/MTDH/LYRIC in liver cancer. Adv Cancer Res 120: 193-221, 2013.

25. Li WF, Dai H, Ou Q, Zuo GQ and Liu CA: Overexpression of microRNA-30a-5p inhibits liver cancer cell proliferation and induces apoptosis by targeting MTDH/PTEN/AKT pathway. Tumor Biol 37: 5885-5895, 2016.
26. Li WF, Ou Q, Dai H and Liu CA: Lentiviral-Mediated short hairpin RNA knockdown of MTDH inhibits cell growth and induces apoptosis by regulating the PTEN/AKT pathway in hepatocellular carcinoma. Int J Mol Sci 16: 19419-19432, 2015.
27. Jiang X, Li W, Tan M, Guo P, Liu X, Pan X, Yu D, Pang Y, Li D, Wang Q, *et al*: Identification of miRNAs involved in liver injury induced by chronic exposure to cadmium. Toxicology 469: 153133, 2022.
28. Ashmawy AM, Elgeshy KM, Abdel Salam ET, Ghareeb M, Kobaisi MH, Amin HAA, Sharawy SK and Abdel Wahab AHA: Crosstalk between liver-related microRNAs and Wnt/β-catenin pathway in hepatocellular carcinoma patients. Arab J Gastroenterol 18: 144-150, 2017.
29. Feng GX, Li J, Yang Z, Zhang SQ, Liu YX, Zhang WY, Ye LH and Zhang XD: Hepatitis B virus X protein promotes the development of liver fibrosis and hepatoma through downregulation of miR-30e targeting P4HA2 mRNA. Oncogene 36: 6895-6905, 2017.
30. Chang N, Ge J, Xiu L, Zhao Z, Duan X, Tian L, Xie J, Yang L and Li L: HuR mediates motility of human bone marrow-derived mesenchymal stem cells triggered by sphingosine 1-phosphate in liver fibrosis. J Mol Med (Berl) 95: 69-82, 2017.
31. Yang CW, Hsu HY, Chang HY, Lee YZ and Lee SJ: 'Natural cardenolides suppress coronaviral replication by downregulating JAK1 via a Na^+/K^+-ATPase independent proteolysis' Biochem Pharmacol 180: 114122, 2020.
32. Morbach H, Schickel JN, Cunningham-Rundles C, Conley ME, Reisli I, Franco JL and Meffre E: CD19 controls Toll-like receptor 9 responses in human B cells. J Allergy Clin Immunol 137: 889-898.e6, 2016.
33. Molinaro A, Becattini B, Mazzoli A, Bleve A, Radici L, Maxvall I, Sopasakis VR, Molinaro A, Bäckhed F and Solinas G: Insulin-Driven PI3K-AKT signaling in the hepatocyte is mediated by redundant PI3Kα and PI3Kβ activities and is promoted by RAS. Cell Metab 29: 1400-1409.e5, 2019.
34. Shariati M and Meric-Bernstam F: Targeting AKT for cancer therapy. Expert Opin Investig Drugs 28: 977-988, 2019.
35. Jamal SME, Alamodi A, Wahl RU, Grada Z, Shareef MA, Hassan SY, Murad F, Hassan SL, Santourlidis S, Gomez CR, *et al*: Melanoma stem cell maintenance and chemo-resistance are mediated by CD133 signal to PI3K-dependent pathways. Oncogene 39: 5468-5478, 2020.
36. Patel KR and Patel HD: p53: An attractive therapeutic target for cancer. Curr Med Chem 27: 3706-3734, 2020.
37. Chao CCK: Mechanisms of p53 degradation. Clin Chim Acta 438: 139-147, 2015.